Evolution of Microstructure and Viscoelasticity during Flow Alignment of a Lamellar Diblock Copolymer

Rangaramanujam M. Kannan and Julia A. Kornfield*

Chemical Engineering 210-41, California Institute of Technology, Pasadena, California 91125

Received July 26, 1993; Revised Manuscript Received November 30, 1993®

ABSTRACT: The effects of flow alignment on the relaxation dynamics of a lamellar diblock copolymer melt and the dynamics of flow alignment itself are investigated using simultaneous measurements of shear stress and birefringence in both the flow plane and the sample plane. The primary advantage of this rheo-optical approach in the context of flow alignment is that it provides quantitative measurements of the evolution of the macroscopic mechanical properties and the state of the microstructure in real time, *in situ* as alignment occurs. Further, it provides information on the molecular and microstructural dynamics that give rise to flow alignment. An entangled, nearly symmetric poly(ethylene–propylene)–poly(ethylethylene) of 50 kg/mol (PEP–PEE-2) is studied during flow alignment under two different conditions, one that enhances alignment of the lamellae parallel to the sample plane and another that induces alignment perpendicular to the sample plane (lamellar normal along the vorticity axis). The results suggest that the flow process leading to parallel alignment in PEP–PEE-2 is associated with inhomogeneous deformation such that the orientation of domains in the material undergoes irreversible "rocking", while the process that produces perpendicular alignment occurs under conditions in which the deformation is nearly homogeneous throughout the material.

1. Introduction

Block copolymers (BCP) are made of sequences of chemically distinct repeat units connected contiguously into chains. They are widely used as adhesives, thermoplastic rubbers, surfactants and compatibilizers,[1] and have been the subject of extensive scientific investigation[2,3] because of their rich thermodynamics, intriguing rheological behavior, and value as model systems for understanding general classes of phase transitions[4] and flow phenomena.[5,6]

In this paper, we focus on the flow behavior of ordered block copolymer melts whose local viscoelastic properties, like colloidal and liquid crystals, are intrinsically anisotropic. Flow fields can be used to introduce a preferred alignment of the microstructure of an ordered BCP, producing materials with highly anisotropic properties.[7–12] Numerous studies of the effect of shear on cylindrical and lamellar-ordered phases have shown that the axes of the cylinders can be aligned along the flow direction, and the normal to the lamellae can be aligned along the velocity gradient direction ("parallel" alignment). Recently, it has been discovered that, simply by changing the flow conditions, the direction of flow-induced alignment in lamellar diblock copolymers can be "flipped" to orient the normal to the lamellae ($\hat{\mathbf{n}}$) along the vorticity axis ("perpendicular" alignment) (Figure 1).[5,6,13,14] This discovery may lead to new applications that use BCP melts as "switchable" materials and has generated renewed interest in understanding the flow alignment of BCP melts.

Although the phenomenon of flow alignment has been known for over two decades,[7] the mechanism is not yet understood. On the basis of the observed changes in microstructural alignment produced by flow, various notions regarding possible mechanisms of alignment have been proposed.[5,9,10,11,13,14] However, a lack of information regarding the dynamic response of the microstructure and macromolecules during flow has made it impossible to discriminate among the concepts put forth in the literature. To address the need for direct observations of the dynamics of flow alignment, we monitor the evolution of the microstructure using simultaneous mechanical and optical measurements. Here, we present the first measurements of stress and birefringence *during* the flow alignment process. The flow response of a lamellar diblock copolymer melt during parallel alignment is compared with its response during the perpendicular alignment process (Figure 1).

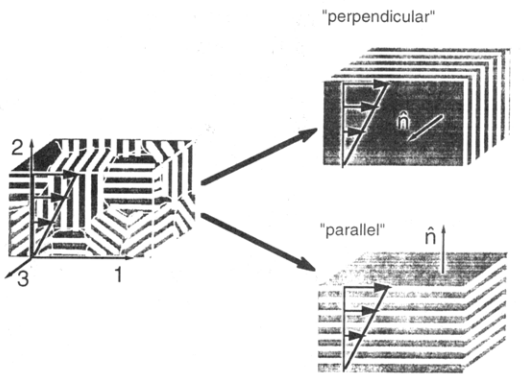

Figure 1. Schematic diagram of the two directions of flow-induced alignment of lamellar block copolymers. "Perpendicular" alignment has been observed in diblock samples subjected to oscillatory shear at temperatures close to the ODT. "Parallel" alignment has been observed in diblock and triblock samples after either steady or oscillatory shear over a wide range of shear rate and temperature. These cartoons are oversimplified: a rich variety of defect structures are observed, and flow enhances a particular direction of alignment rather than perfecting it (see electron micrographs and scattering patterns[5,13]).

We begin by reviewing the previous experimental studies, the conceived mechanisms of flow alignment that motivate our research, and the basis for using birefringence measurements to characterize evolution of the microstructure during flow alignment. Next, we describe the model polymer, apparatus, and methods used in this study. Section 4 presents the results of dynamic stress and birefringence measurements, characterizing both the effects of flow alignment on the dynamics of a BCP melt and the development of flow alignment as it occurs. We conclude by discussing the implications of these results and directions for future work.

® Abstract published in *Advance ACS Abstracts,* February 1, 1994.

0024-9297/94/2227-1177$04.50/0

2. Background

The phase behavior of diblock (A–B) copolymers in the bulk are largely determined by two factors: χN and f, where χ is the A–B segment–segment interaction parameter, N is the overall length of the polymer, and f is the fraction of the A component.[2] When the repulsive interaction ($\sim\chi N$) is sufficiently weak, entropy dominates and the polymer exists in a compositionally-disordered phase. As χN increases, the repulsive interactions favor a reduction in the number of A–B contacts. Above a critical value of χN, the two blocks segregate into ordered microstructures. This transition is referred to as the order–disorder transition (ODT). The morphology of the ordered microstructure depends on f. When the BCP orders, the orientation of the principal axes of the microstructure vary with position in the sample, and various defects are trapped in the material.[12-14] In the absence of a symmetry-breaking field, the ordered material is isotropic on a macroscopic scale.[7,10]

2.1. Flow-Induced Alignment. While a preferred orientation can be introduced by electric fields[15] or surface effects,[16] flow provides the most potent means to manipulate the macroscopic alignment of the microstructure of ordered block copolymers.[5,7-12] Flow-induced alignment of BCPs was discovered in a styrene–butadiene–styrene (SBS) triblock copolymer with a cylindrical ordered morphology.[7,8] Subsequently, it was shown that oscillatory shear is effective in orienting cylindrical and lamellar-ordered phases of block copolymers.[9] The resulting alignment of the cylinders was found to be along the flow direction. Lamellae were found to align normal to the velocity gradient.

To explain flow alignment, Hadziioannou *et al.*[9] offered the following concepts regarding possible mechanisms: selective rotation of "grains" in the material, selective melting of grains, and defect migration. Selective rotation is hypothesized to lead to a progressive alignment of grains along the direction that minimizes their resistance to flow. Selective melting was suggested to produce alignment by selectively disordering domains in which the microstructure is oriented in "unfavorable" directions. Indeed, in a shear flow, there is a "least favorable" alignment: lamellae oriented broadside to the flow would experience layer compression if they deformed affinely. Layers oriented edge-on to the flow can shear without layer compression. Thus, regions with layers broadside to the flow are relatively rigid and more likely to be subjected to destabilizing distortions.[17] Finally, defect migration was added as a mechanism for grain boundaries to anneal out of the material once the grains themselves had been aligned. Without any information on the dynamics of flow alignment itself, it has not been possible to test the validity of these general notions, nor to develop a more precise description of the actual mechanism of flow alignment.

The quest for a mechanism for flow alignment became a search for at least two mechanisms when Koppi *et al.*[5] discovered that the direction of orientation of lamellar diblock copolymers is not always along the flow direction (parallel), but could be flipped 90° (Figure 1) by changing the flow conditions. This behavior was found to be restricted to temperatures near the ODT and to frequencies that were slow when compared to molecular relaxation, but fast when compared to some critical frequency. The precise limits of the perpendicular regime are not yet known. Shearing the sample just above the ODT can induce ordering, and the lamellae form aligned along the perpendicular direction.[6] Regarding the mechanism that produces perpendicular alignment, the observation that this orientation is found only near the ODT suggests that fluctuations play a key role.[18] Perpendicular alignment has since been observed in a polystyrene–polyisoprene (12.5k–9.5k, denoted SI 12/9) lamellar diblock, also at frequencies that are slow compared to macromolecular relaxation and at temperatures close to the ODT.[14] A regime of parallel alignment at frequencies below those producing perpendicular alignment has been observed in PEP–PEE-2; in contrast, SI 12/9 is driven toward parallel alignment at sufficiently high shear frequencies.[13] Together, these observations suggest that three different mechanisms of flow alignment may exist and that entanglement, viscoelastic contrast between the lamellae, and the strength of order are likely to be important factors in determining the flow behavior of BCPs.

The first steps toward investigating the evolution of flow alignment were taken by Morrison *et al.*,[10,11] who examined samples of a styrene–butadiene–styrene (SBS) triblock with cylindrical morphology quenched at intermediate states of alignment. On the basis of their observations, they proposed that below a critical stress flow alignment occurred due to the flow of "grains" such that the domains are not disrupted and may flow as a unit; above the critical stress, flow alignment occurred by selective melting or by a combination of the flow of grains and selective melting. Their results reinforce questions that have persisted in the literature regarding the microrheology of flow alignment, its dependency on proximity to the ODT, proximity to the glass transition of one or both blocks, and shear rate or shear stress.

To address the need for information on the dynamics of block copolymers during flow alignment, one requires experimental methods to characterize the changes in the microstructure induced by flow, and their relationship to changes in the macroscopic viscoelastic properties of the material. Rheooptical methods are particularly well suited to observe the development of alignment of the ordered structures in BCPs, and the molecular and microstructural responses that lead to it. The general principle behind optical rheometry is to use the connection between the state of the microstructure of a fluid and the observable anisotropies in its optical properties.[19] In this study we take advantage of the relationship between BCP microstructure and anisotropy in the real part of its refractive index, or birefringence.

2.2. Flow Birefringence of Block Copolymers. The birefringence of a quiescent, ordered block copolymer carries information about the orientation distribution of the microstructure. Two contributions can be distinguished: the tendency of the chains to align perpendicular to interfaces in the material (intrinsic birefringence) and the anisotropy of the phase-separated microstructure (form birefringence). *Both* contributions are coaxial, so that the principal axes of the refractive index tensor coincide with those of the ordered structure.[20] Thus, in a sufficiently weak flow that the conformation of the chains is not significantly distorted from equilibrium, the birefringence of a lamellar block copolymer provides a means to measure the second moment of the orientation distribution of the layer normal.

In a quiescent homopolymer melt, all orientations of the end-to-end vector are equally probable and the polymer is optically isotropic. When subjected to stress, the melt flows and the conformation of the chains is perturbed. The bias in the orientation distribution of chain segments is manifested in anisotropic optical properties. For homopolymer melts and concentrated solutions over a wide range of flow conditions, birefringence is related to stress by the stress–optical rule: the deviatoric parts of the stress tensor and the refractive index tensor are proportional to each other.[21]

Ordered block copolymers can be birefringent even at rest. Therefore, the stress–optical rule cannot be valid in general. Nevertheless, under flow conditions that perturb the chain conformations significantly from that dictated by the microphase structure, the stress and birefringence might both be dominated by the contributions associated with the distortion of the chain conformation. This is most likely to be the case when the time scale of the flow is rapid compared to conformational relaxation. In this regime, the stress can be expected to disturb the segmental orientation distribution of the molecules, producing a contribution to intrinsic birefringence. If this contribution dominates over the birefringence associated with the microstructure, the stress–optical rule would hold in this regime of rapid deformation. As the time scale of the flow slows, the birefringence associated with the microstructure becomes increasingly important relative to the birefringence arising from the distortion of chain conformation, and there is no reason to expect the stress–optical rule to hold. Therefore, it is of interest to examine the conditions for applicability of the stress–optical rule to block copolymers and the way the stress–optical rule fails when it does.

Previous studies of flow alignment motivate us to investigate the mechanisms that lead to parallel and perpendicular alignment. In order to achieve this, we monitor the evolution of the microstructure by measuring stress and birefringence before, during, and after the alignment process. While stress is sensitive to the macroscopic response, birefringence is sensitive to both the molecular and microstructural responses. Here we show that, together, they provide insight regarding the mechanism of flow alignment.

3. Experimental Section

3.1. Material. The polymer used in this study is a nearly symmetric poly(ethylenepropylene)–poly(ethylethylene) diblock copolymer of M_w = 50 100 g/mol (PEP–PEE-2) synthesized by Bates.[22] The synthesis, characterization, and viscoelastic properties of this polymer have been described previously by Bates and co-workers.[22,23] It possesses good thermal and oxidative stability, a readily accessible ODT (T_{ODT} = 96 °C), blocks that are long enough to be entangled, and a narrow molecular weight distribution (M_w/M_n = 1.07). "Flipping" was discovered in PEP–PEE-2D, the partially deuterated counterpart of the present material.[5] It has been shown that when PEP–PEE-2 is subjected to prolonged oscillatory shear at T/T_{ODT} = 0.97 with 100% strain amplitude, a shear frequency ω = 0.02 rad/s enhances parallel alignment, whereas ω = 1 rad/s produces perpendicular alignment.[5]

3.2. Apparatus. The mechanical and stress–optical properties of this block copolymer were characterized using a rheo-optical apparatus developed in our laboratory. The center of the apparatus is the Rheometrics RSA-II dynamic mechanical testing system, which was modified to permit optical measurements. Dynamic birefringence was measured using a polarization–modulation scheme (optical train, Figure 2a).[24] This rheo-optical apparatus is described in detail elsewhere.[25,26] It is uniquely suited for simultaneous, quantitative measurements of dynamic stress and birefringence over a wide range of frequency (0.01–100 rad/s) and temperature (−100 to +400 °C).

Rheo-optical experiments were performed using the "shear-sandwich" geometry, with the optical axis either along the velocity gradient direction or along the vorticity direction (Figure 2b), thus enabling us to probe two different projections of the anisotropic refractive index tensor. This is particularly useful because the projection that is most sensitive to the evolution of the microstructure depends on the direction of the lamellar alignment. Birefringence in the 1,2-plane or 1,3-plane is measured with the optical axis along the vorticity direction (axis 3, Figure 2b) or the velocity gradient direction (axis 2, Figure 2b), respectively. The parallel plate devices used in all of the experiments reported here (Figure 2) have gaps of 0.5 mm and

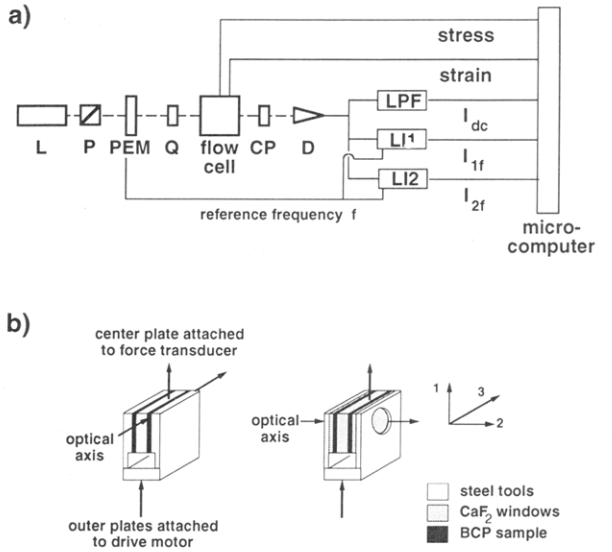

Figure 2. (a) Rheo-optical apparatus for simultaneous measurement of dynamic shear stress and birefringence. The instrument consists of an HeNe laser (wavelength λ = 633 nm) (L), linear polarizer (P), photoelastic modulator (PEM), quarter-wave plate (Q), shear sandwich flow cell in the Rheometrics Solids Analyzer RSA-II, circular polarizer (CP), and detector (D). The signal from the detector is analyzed using a low-pass filter and two lock-in amplifiers: one at the first harmonic ($1f$) and the other at the second harmonic ($2f$) of the modulator frequency. (b) Two shear sandwich flow cells are used. The conventional tool made by Rheometrics (left) is used for measurements of birefringence in the 1,2-plane. A custom tool (right) is used for measurements in the 1,3-plane.

plates of 2 cm² area (15.95 mm × 12.65 mm). For optical measurements in the 1,3-plane, custom shear-sandwich fixtures were made with the plates replaced by CaF_2 windows. In this case, the optical path length was twice the gap width, *i.e.* 1.0 mm.

The signals from the displacement and force transducers, the low-pass filter (I_{dc}), and two lock-in amplifiers at the fundamental f and the second harmonic $2f$ of the modulator (I_{1f} and I_{2f}) are recorded using a microcomputer. The strain, stress, $R_{1f} \equiv I_{1f}/I_{dc}$, and $R_{2f} \equiv I_{2f}/I_{dc}$ are calculated from these results. For a sample with zero dichroism and having a principal axis of birefringence oriented at an angle α with respect to the flow direction, the ratios R_{2f} and R_{1f} are related to the retardance μ of the sample by $R_{2f} = 2J_2(A) \sin \mu \sin 2\alpha$ and $R_{1f} = -2J_1(A) \sin \mu \cos 2\alpha$, where $J_1(A)$ and $J_2(A)$ are Bessel functions of the first and second order evaluated at the amplitude of the modulator (A) and $\mu = (2\pi d/\lambda)\Delta n_{ij}$, with d the optical path length, λ the wavelength of the incident light, and Δn_{ij} the birefringence in the i,j-plane (1,2- or 1,3-plane in our work). From $R_{1f}(t)$ and $R_{2f}(t)$, we calculate $\Delta n_{ij}(t)$ and $\alpha(t)$. The Fourier transforms of the time domain signals are calculated. The relevant Fourier components are the fundamental (1ω) of the strain, stress, and $\Delta n_{ij} \sin 2\alpha$ and the dc component of $\Delta n_{ij} \cos 2\alpha$, as is explained below.

3.3. Stress and Birefringence in BCPs. In shear flow with the coordinate system of Figure 1, the stress tensor has the following nonzero terms:

$$\sigma = \begin{bmatrix} \sigma_{11} & \sigma_{12} & 0 \\ \sigma_{12} & \sigma_{22} & 0 \\ 0 & 0 & \sigma_{33} \end{bmatrix} \quad (1)$$

By symmetry we expect the shear stress σ_{12} to be an odd function of the strain, and the normal stress differences $N_1 = \sigma_{11} - \sigma_{22}$ and $N_2 = \sigma_{22} - \sigma_{33}$ to be even functions of the strain. In the case of oscillatory shear $\gamma(t) = \gamma_o \sin \omega t$, if γ_o is small we expect only the leading terms to dominate. Thus, σ_{12} is expected to be sinusoidal with the same frequency as the applied strain. While flow certainly can perturb the microstructure and consequently the viscoelastic properties of block copolymer melts, there may exist sufficiently small strain amplitudes that the complex amplitude of the stress oscillation is linear in the strain and independent of time during prolonged shear. When this is the case we can

define storage and loss moduli, $G'(\omega)$ and $G''(\omega)$, for the block copolymer that depend on temperature and on the previous (large amplitude) flow history of the material:

$$\sigma_{12} = \gamma_o[G' \sin \omega t + G'' \cos \omega t] \quad (2)$$

There may exist an intermediate range of γ_o for which the shear stress can be described in terms of effective dynamic moduli G^*_{eff}, which change with time during prolonged shear due to flow-induced changes in fluid structure.[27]

We restrict ourselves here to sufficiently small strains that the shear stress is simply sinusoidal at the frequency ω. We perform two types of experiments. One type ("frequency sweep") uses such a small strain amplitude that no change in viscoelastic properties is observed even after completing experiments over a wide range of frequency. The second type ("flow alignment") uses strain amplitude large enough to produce alignment of the lamellae, but with small enough strain that the stress can be described using G^*_{eff}, which is monitored as a function of time during prolonged shearing.

In a shear flow, the refractive index tensor $\mathbf{n}$ has a form similar to the stress tensor:

$$\mathbf{n} = \begin{bmatrix} n_{11} & n_{12} & 0 \\ n_{12} & n_{22} & 0 \\ 0 & 0 & n_{33} \end{bmatrix} \quad (3)$$

Regarding the birefringence, we are concerned with two particular projections of $\mathbf{n}$. The projection on the 1,2-plane, $\mathbf{n}_{12}$, is observed when the optical axis coincides with the vorticity axis:

$$\mathbf{n}_{12} = \begin{bmatrix} n_{11} & n_{12} \\ n_{12} & n_{22} \end{bmatrix} \quad (4)$$

The magnitude of the birefringence in the 1,2-plane, Δn_{12}, is equal to the difference between the principal eigenvalues of $\mathbf{n}_{12}$. In terms of the experimentally observed Δn_{12} and orientation angle α of the principal axis of $\mathbf{n}_{12}$ with respect to the flow direction,

$$n_{12} = \frac{1}{2}\Delta n_{12} \sin(2\alpha) \quad (5)$$

and

$$n_{11} - n_{22} = \Delta n_{12} \cos(2\alpha) \quad (6)$$

The projection of $\mathbf{n}$ on the 1,3-plane, $\mathbf{n}_{13}$, is probed when the optical axis is along the velocity gradient. The principal axes of $\mathbf{n}_{13}$ coincide with axes 1 and 3 (*i.e.*, $\alpha = 0$), so its anisotropy is completely described by the magnitude of the birefringence $\Delta n_{13} = n_{11} - n_{33}$.

Neglecting the symmetry breaking involved in the choice of the initial and final shearing directions, we expect similar small strain regimes for n_{12} as for σ_{12}. We define a complex birefringence coefficient $B^* = B' + iB''$ for n_{12} by[28]

$$n_{12} = \gamma_o[B' \sin \omega t + B'' \cos \omega t] \quad (7)$$

Like the shear stress, there may exist a regime of sufficiently small strain that B^* is simply a function of the shear frequency and the state of the microstructure. At somewhat larger strains, the effect of oscillatory shear on the microstructure of the fluid may be manifested in changes in the dynamic birefringence with time, which can be described by $B^*_{eff}(t)$.[27]

Again, neglecting the symmetry breaking involved in choosing an initial flow direction, one does not expect n_{12} to build up due to oscillatory shear (*i.e.* it will oscillate about zero). Consequently, if a particular orientation of the projection of the lamellar normal in the 1,2-plane were enhanced by oscillatory shear, it would be directed along one of the axes (1 or 2) and would be manifested in $n_{11} - n_{22}$. Similarly, if a particular orientation of the projection of the lamellar normal in the 1,3-plane tends to be aligned by flow, it will be manifested in $n_{11} - n_{33}$. Thus, the evolution of the steady offset in $n_{11} - n_{22}$ and $n_{11} - n_{33}$ is sensitive to the development of alignment.

Table 1. Shift Factors and Effective Stress-Optic Coefficients of PEP-PEE-2

T (°C)	a_T	b_T	$b_{T,so}$	$10^{10}C_{eff}$ (cm²/dyn)
22	380	1.34	1.07	1.5_6
45	35	1.20	1.02	1.4_9
65	5.4	1.09	1.00	1.3_5
87	1	1	1	1.2_4

To characterize the relative magnitude of the birefringence compared to stress, we define three stress-optic ratios based on the magnitude, the real part, and the imaginary parts of the complex birefringence coefficient and the dynamic modulus:

$$\mathrm{SOR} = \frac{|B^*|}{|G^*|} \quad (8)$$

$$\mathrm{SOR}_{Re} = \frac{B'}{G'} \quad (9)$$

$$\mathrm{SOR}_{Im} = \frac{B''}{G''} \quad (10)$$

For homopolymer melts, under the relatively mild flow conditions of interest here, the stress-optical rule would hold and SOR, SOR_{Re}, and SOR_{Im} would be independent of frequency and all equal to the stress-optic coefficient, C. For BCPs, the specific way in which the stress-optical rule breaks down may offer clues regarding microstructural dynamics. Examining the stress-optical behavior using these ratios exposes different regimes of flow response in terms of the relationship between molecular/microstructural orientation and stress.

3.4. Methods. Two types of oscillatory shear protocols were used, as described above: (1) frequency sweeps at small-strain amplitudes (≤9%) to characterize the state of the sample before and after alignment, and (2) prolonged, large amplitude (roughly 100%) oscillatory shear at a fixed frequency to induce macroscopic alignment of the microstructure. Stress and birefringence were recorded simultaneously during both types of experiments.

We report rheo-optical measurements during the flow alignment process at two different frequencies at 87 °C and 90% strain: (1) at 0.02 rad/s for 92 cycles, and (2) at 1 rad/s for 1800 cycles. As mentioned above, similar conditions have previously been shown to produce parallel and perpendicular alignment, respectively.[5] To establish a reproducible initial condition before each alignment experiment, the sample was heated well into the disordered phase (135 °C) and allowed to equilibrate at that temperature for 25 min. The sample was then cooled to the desired temperature in the ordered state and allowed to equilibrate for 25 min. This procedure resulted in a reproducible unaligned initial state, confirmed by the rheo-optical measurements before and during the alignment process.

4. Results

4.1. Stress-Optical Properties before and after Alignment. The dynamic moduli and complex birefringence coefficient were measured at 22, 45, 65, and 87 °C using small amplitude oscillatory shear. Frequency-sweep experiments were performed first on the unaligned BCP and then on the aligned states obtained by prolonged oscillatory shear. The aligned state of the material was designated "parallel" after 7 h of shearing at $\gamma_o = 90\%$ and $\omega = 0.02$ rad/s at 87 °C (similar to the conditions that produced parallel alignment as indicated by SANS[5]). It was designated "perpendicular" after 2.5 h of shearing at $\gamma_o = 90\%$ and $\omega = 1$ rad/s (again based on previous SANS results[5]).

The dynamic moduli (G^*) measured at different temperatures ($T \leq 87$ °C) could be superimposed by using appropriate shift factors (Table 1). The frequency (a_T) and vertical (b_T) shift factors are very close to the values reported previously.[23] A master curve for the dynamic birefringence (B^*) is obtained with identical frequency shift factors, but with slightly different vertical shift factors

($b_{T,so}$ in Table 1) due to the temperature dependence of the effective stress–optic coefficient, described below.

The dynamic birefringence and dynamic modulus master curves of the unaligned BCP are compared in Figure 3. At high reduced frequencies, the dynamic birefringence and dynamic modulus may be superimposed by dividing B^* by an effective stress–optic coefficient C_{eff}. This shifted dynamic birefringence is denoted as G^*_{so}. At all accessible frequencies at 22 and 45 °C, SOR_{Re} and SOR_{Im} are constant and equal to each other, leading to the values of C_{eff} given in Table 1. At 65 and 87 °C, C_{eff} is calculated using the results at high enough frequencies that SOR_{Re} and SOR_{Im} are independent of frequency and equal to each other. The temperature dependence of C_{eff} is in accord with that observed for PEP homopolymer melts[25] and accounts for the difference in vertical shift factors for G^* and B^* (Table 1).

Thus, the stress–optical rule appears to hold above a critical frequency. With decreasing frequency, deviations from the stress–optical rule are first evident in the elastic-like character (G' and G'_{so}), below a critical frequency $\omega'_{c,so}$. Deviations are evident in the loss-like behavior (G'' and G''_{so}) only at much lower frequency, below $\omega''_{c,so}$. Both of these are at least an order of magnitude smaller than the frequency where the storage and loss moduli cross (ω_x).

The dynamic moduli and birefringence are modified by flow alignment. In the low-frequency regime where viscoelastic properties are sensitive to the order–disorder transition,[23] the dynamic moduli of PEP–PEE-2 are reduced by flow alignment (Figure 4). The dynamic moduli observed using $\gamma_o \leq 2\%$ are in agreement with those reported previously,[5] for both the perpendicular- and parallel-aligned states. For comparison with earlier work, the critical frequencies, below which the storage and loss moduli are sensitive to the ordering transition, are indicated by ω'_c and ω''_c, respectively (Figure 4). At the lowest reduced frequencies, we resorted to using a higher strain (9%), which was accompanied by a noticeable decrease in the storage modulus.

The way that the stress–optical rule fails at low frequency (Figure 3) is also modified by flow alignment. In particular, the regime in which the stress–optical rule appears to hold extends to lower frequency in flow aligned states (Figure 5). For the unaligned material, SOR is constant at high enough frequencies (above $\omega_{c,so} \approx 2$ rad/s, consistent with the results shown in Figure 3). Below this frequency the birefringence per unit stress increases with decreasing frequency. Although the results in this regime do not cover a wide dynamic range, they suggest that there may be a power law regime ($\sim\omega^{-1/2}$ is shown for comparison in Figure 5). The two aligned states have similar SOR(ω), each with a critical frequency that is 1 order of magnitude smaller than that observed for the unaligned state.

4.2. Stress–Optical Behavior during Parallel Alignment. During prolonged large amplitude shear at 0.02 rad/s at constant strain amplitude, the magnitudes of the σ_{12} and n_{12} oscillations decrease and a displacement develops in $n_{11} - n_{22}$ (Figure 6). The decrease in the amplitude of the oscillation of n_{12} is more dramatic than that of σ_{12}. The magnitude and time scale of the growth of the displacement of $n_{11} - n_{22}$ appear to be correlated with the magnitude and rate of the decrease in the amplitude of n_{12}.

Both σ_{12} and n_{12} oscillate with the same frequency as the applied strain. Thus, they can be described in terms of complex coefficients $G^*_{eff}(t)$ and $B^*_{eff}(t)$. The effective storage and loss moduli (Figure 7a) decrease over 7 h of shearing, but the decay in G'_{eff} is more pronounced than that of G''_{eff}. For reference, the moduli observed at 9% strain at the same frequency are indicated by arrows. During the parallel alignment process B^*_{eff} decreases more strongly than G^*_{eff}, with B'_{eff} falling by 1 order of magnitude and B''_{eff} dropping by a factor of 4 (Figure 7b). Thus, the relative magnitude of the birefringence compared to the stress, SOR, decreases significantly, and this decrease is associated with the elasticlike response of the material SOR_{Re} (Figure 7c).

4.3. Stress–Optical Behavior during Perpendicular Alignment. The development of perpendicular alignment is monitored in a similar way, with the distinction that the displacement of the birefringence in the 1,3-plane is recorded to monitor the progressive alignment of the lamellae. The shear stress and birefringence n_{12} are again described by $G^*_{eff}(t)$ and $B^*_{eff}(t)$ (Figure 8). The loss-like character (G''_{eff} and B''_{eff}) is almost unchanged as alignment progresses. During the first 3000 s, G'_{eff} and

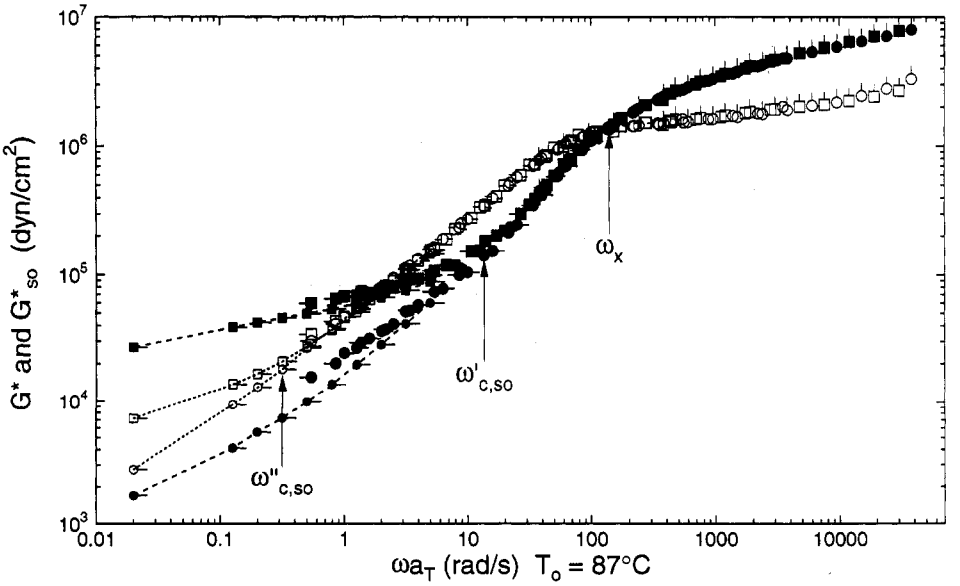

Figure 3. Dynamic moduli (G^*) and complex birefringence coefficient scaled by the effective stress-optic coefficient (see text) (G^*_{so}) of unaligned PEP–PEE-2: G' (●), G'' (○), G'_{so} (■), G''_{so} (□). Data at 22 °C are designated by a vertical arm, 45 °C by no arm, 65 °C by a left arm, and 87 °C by a right arm. Larger symbols indicate results at strain amplitude $\gamma_o < 2\%$; smaller symbols connected by dashed lines indicate results with $\gamma_o = 9\%$.

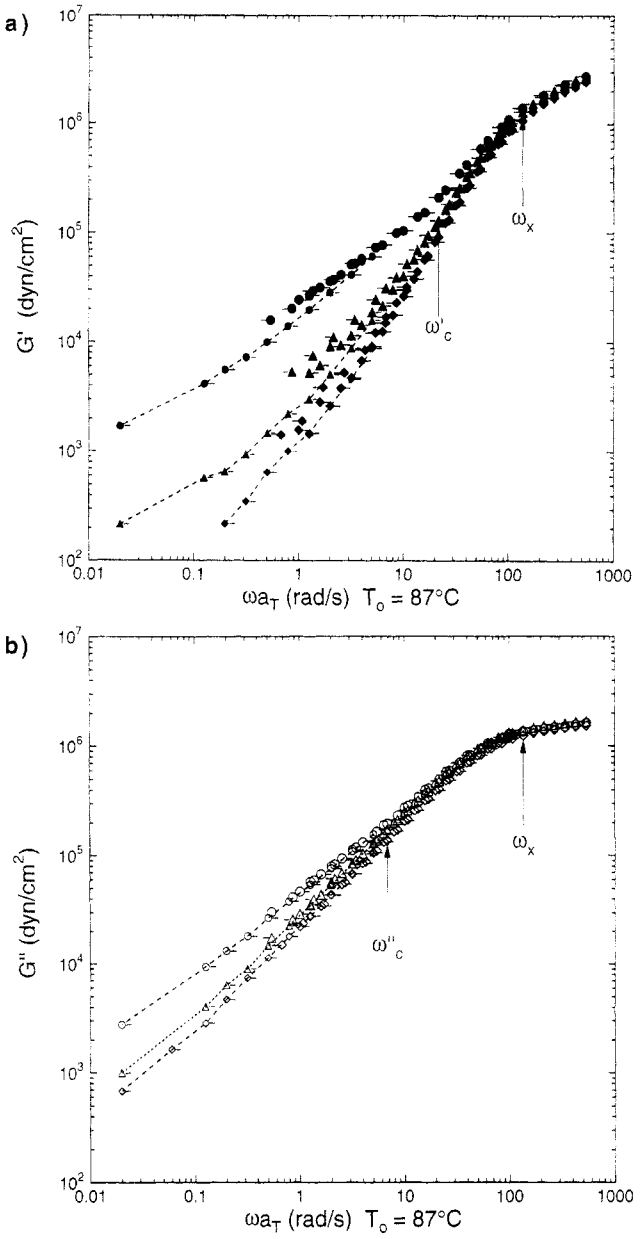

Figure 4. Storage moduli (a) and loss moduli (b) of unaligned (● and ○), "parallel" (solid and open Δ) and "perpendicular" (solid and open ◊) aligned PEP–PEE-2. Data at 65 °C are designated by a left arm and at 87 °C by a right arm. Larger symbols indicate results at strain amplitude $\gamma_o < 2\%$; smaller symbols connected by dashed lines indicate results with $\gamma_o = 9\%$.

B'_{eff} decrease together. The monotonic development of perpendicular alignment is manifested in the displacement component of $n_{11} - n_{33}$ (Figure 8c). The sharp increase in $|(n_{11} - n_{33})(d)|$ during the first 200 s coincides with the period when most of the decrease in G'_{eff} and B'_{eff} occurs. Nevertheless, the displacement $|(n_{11} - n_{33})(d)|$ doubles over the next 4000 s, while G'_{eff} decreases only 25% and B'_{eff} becomes erratic.

5. Discussion

5.1. Dynamics of the Unaligned, Lamellar Melt. Comparison of the dynamic shear stress and birefringence in the ordered but unaligned BCP melt reveals a frequency regime where the stress–optic rule appears to hold ($\sigma_{12} \propto n_{12}$) (Figure 3). Since the form birefringence is negligible compared to the intrinsic birefringence in PEP–PEE diblock copolymers,[20] the birefringence reveals the segmental orientation of the chains. In the regime where σ_{12}

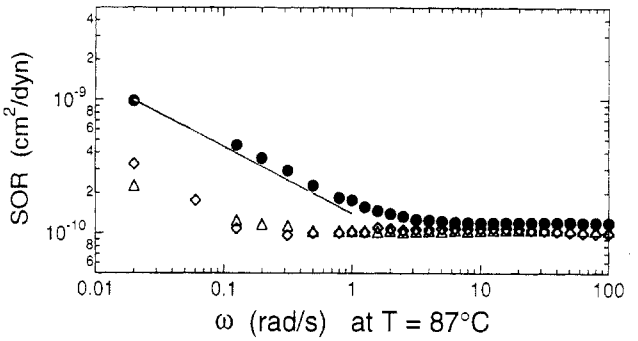

Figure 5. Effect of flow alignment on the amplitude-based stress–optic ratio SOR of PEP–PEE-2 in unaligned (●), "parallel" (Δ), and "perpendicular" (◊) states. For reference, the line shows a $\omega^{-1/2}$ power law.

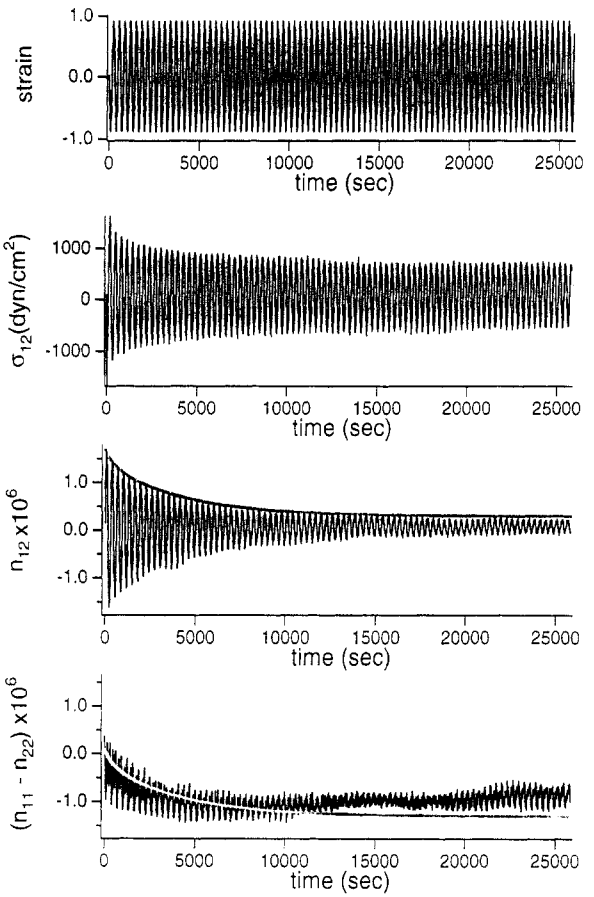

Figure 6. Behavior of the shear stress and birefringence in the 1,2-plane (both n_{12} and $n_{11} - n_{22}$) during 80 cycles of sinusoidal shear of $\gamma_o = 90\%$ at $T = 87$ °C. Similar conditions have been shown to enhance "parallel" alignment. The black curves connect the data points. The heavy gray curve approximates the envelope of the decaying oscillation of n_{12}. It is also shown on the graph of $n_{11} - n_{22}$ for comparison.

$\propto n_{12}$, both the shear stress and the dynamic birefringence n_{12} are primarily associated with the distortion of chain conformation. Indeed, this behavior is confined to frequencies near and above the terminal molecular relaxation time ($\omega \geq 1/4\omega_x$). As frequency decreases, there is a crossover to a regime where the relative magnitude of n_{12} with respect to σ_{12} increases with decreasing frequency. This crossover occurs first in the storage components (G' and B'), as the elastic character associated with the relaxation of entanglements becomes less significant than the elasticity associated with the microstructure. In unaligned PEP–PEE-2, G' and G'_{so} diverge below a critical frequency $\omega'_{c,so}$ that is only slightly lower than ω'_c (the frequency below which G' is sensitive to the ordering transition). The critical frequency $\omega''_{c,so}$ below

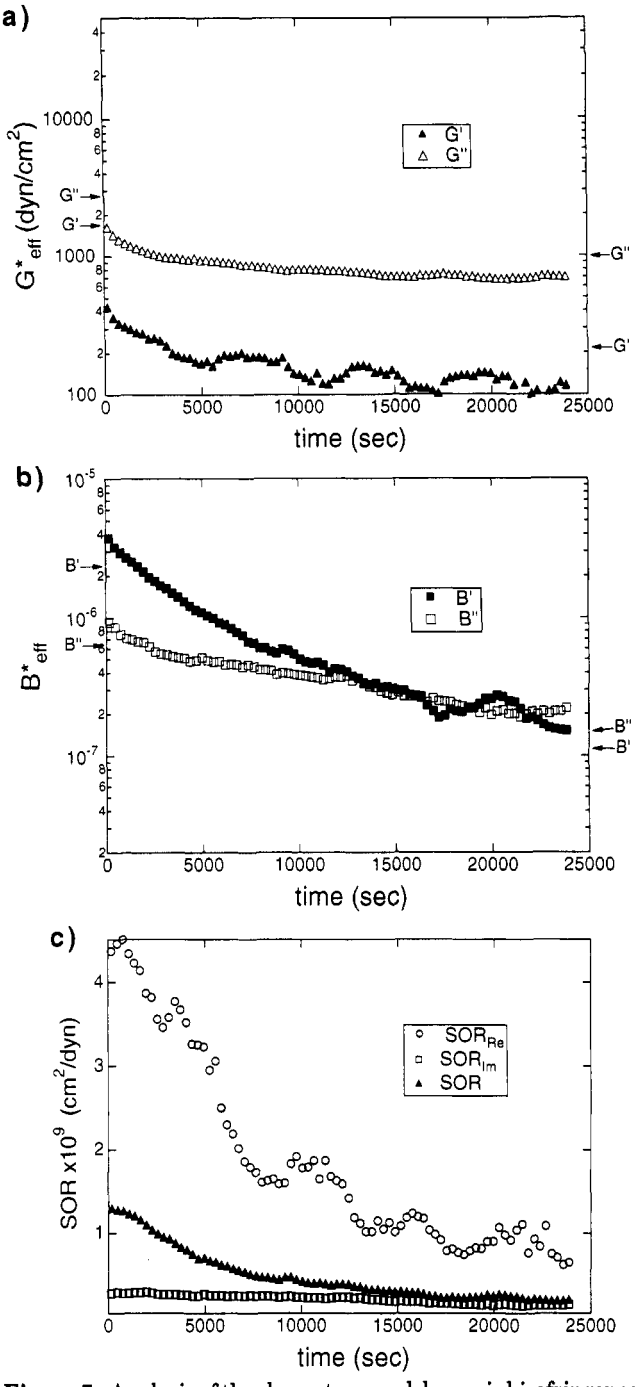

Figure 7. Analysis of the shear stress and dynamic birefringence n_{12} during the "parallel" flow alignment process (Figure 6) in terms of (a) effective dynamic moduli, (b) the effective complex birefringence coefficient, and (c) the amplitude-based stress–optic ratio SOR. The arrows at the left and right edges of the graphs in parts a and b indicate the values of the dynamic moduli and birefringence coefficient observed at 0.02 rad/s with small strain (9%). The arrows on the left show values for the unaligned material; those onthe right are for the parallel aligned state.

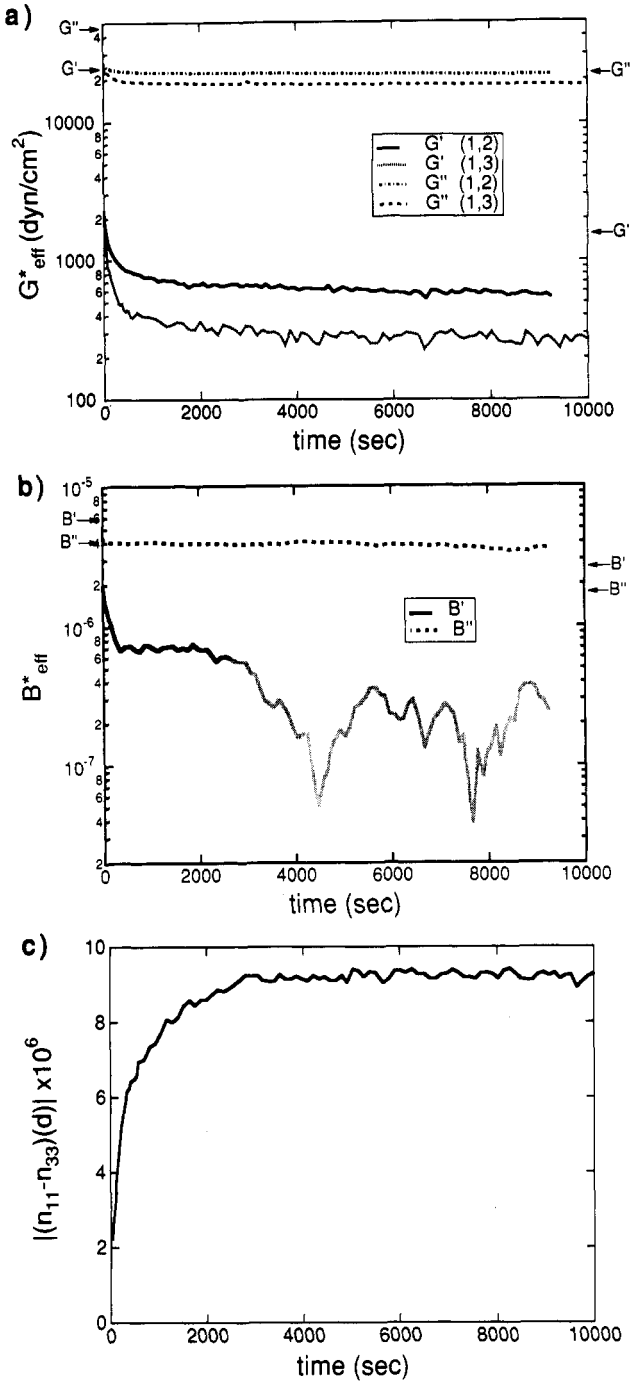

Figure 8. Evolution of shear stress and birefringence during the "perpendicular" flow alignment process: (a) effective dynamic moduli, (b) effective complex birefringence coefficient, and (c) magnitude of the displacement component of the birefringence in the 1,3-plane ($n_{11} - n_{33}$). The arrows at the left and right edges of the graphs in parts a and b indicate the values of the dynamic moduli and birefringence coefficient observed at 1 rad/s with small strain (1%).

which the loss-like character shows deviations between G'' and G''_{so} is far below not only $\omega'_{c,so}$ but also ω''_c. Its value corresponds to ω_d reported by Koppi *et al.*[5] in unaligned, ordered PEP–PEE-2 and which they associated with defect motions ($\omega_d a_T \approx 0.4$ rad/s for $T_o = 87$ °C). We believe that the regime between $\omega'_{c,so}$ and $\omega''_{c,so}$ is that in which the viscoelastic response is governed by the layered structure in the material, as described below.

Just below ω'_c and ω''_c there is a power law region where $G' \sim G'' \sim \omega^{0.7}$, as has been reported previously.[23] This type of behavior, intermediate between a solid and liquid, appears to be characteristic of layered liquids in general.[30] Kawasaki and Onuki have shown that for a layered liquid with modulus B for layer compression, viscosity η_o and isotropic distribution of lamellar orientation, at frequencies below a critical frequency $\omega_c \equiv B/\eta_o$ the dynamic moduli are $G' \approx G'' \approx (\pi/24\sqrt{2})(B\eta_o\omega)^{1/2}$.[31] This regime is cut off at low frequency by the contributions of defect structures. If the layer spacing is λ_s and the typical distance between defects is l_D, then this lower-frequency crossover is anticipated at $\omega(\lambda_s/l_D)^2$. Extending this analysis to the stress–optical behavior, Milner and Fredrickson have shown that in this intermediate range of frequencies where the layer structure dominates the viscoelasticity, the stress–optic ratio should scale as SOR $\sim \omega^{-1/2}$.[32] This scaling is in agreement with the observed SOR (ω) (Figure 5).

This theoretical picture explains the existence of an intermediate range of frequency in which the viscoelastic relaxation shows power law behavior. In this region it is anticipated that the stress–optic rule will fail, with a power law dependence of SOR. This regime is limited on the high-frequency side by the domain in which the viscoelasticity is dominated by molecular relaxation, and on the low-frequency side by the contribution of the larger-scale structure (presumably focal conic defects and grain boundaries).[12-14] Our results provide strong support for this physical picture of the dynamics of an unaligned, lamellar BCP melt.

5.2. Effect of Alignment on Dynamics. Stress–optical measurements on aligned samples show that the frequency regime in which the stress–optical rule appears to hold extends to lower frequencies in aligned samples than in unaligned PEP–PEE-2 (Figure 5). Since the dynamics that enhance SOR at low frequency are eliminated by alignment, the deviations from the stress–optical rule are associated with inhomogeneous orientation and/or defect structures trapped in an unaligned or partially aligned BCP. This is reasonable, since a sample with perfect lamellar alignment, in either the parallel or the perpendicular orientation, subjected to oscillatory shear of $\gamma_o \leq 100\%$ would not experience significant distortion of the layer spacing or curvature. Thus, the shear stress and n_{12} would be primarily associated with the distortion of the conformation of the polymers, and the stress–optical rule would be expected hold for n_{12} and σ_{12} in an ideal, aligned BCP.

With respect to the oscillatory shear conditions used to induce alignment, the perpendicular alignment has the smaller dynamic moduli at both of the frequencies used for flow alignment (Figure 4). Thus, the simple notion that the system adjusts itself to minimize its resistance to flow[9] cannot describe the "flipping" of alignment direction that is observed in PEP–PEE-2. Instead, it is likely to be dictated by a change in the time scale of the flow with respect to a characteristic time scale of the BCP dynamics.[5] Among the characteristic frequencies exhibited by the unaligned BCP ($\omega'_{c,so}$, $\omega''_{c,so}$, ω'_c, ω''_c and ω_x), the one that lies between the frequency used to produce parallel alignment (0.02 rad/s) and that used for perpendicular alignment (1 rad/s) is $\omega''_{c,so}$. Here, it is tempting to speculate that the mechanism of parallel alignment overcomes that of perpendicular alignment when the viscoelastic behavior is dictated by microstructural dynamics (*i.e.*, $\omega < \omega''_{c,so}$). At higher frequencies and near the ODT, the mechanism that leads to perpendicular alignment dominates, perhaps due to the dynamics of the lamellar structure manifested by $\omega'_{c,so}$. At yet higher frequencies ($\omega > \omega_x$) that only probe chain entanglement, it is likely that another regime of behavior will be found; we expect no alignment to occur there, because the excited modes are so local and the viscoelastic properties of PEP and PEE are so similar. Certainly, further experiments are required to identify crossover frequencies between different regimes of behavior and their relationship to the characteristic frequencies of the BCP.[33]

In generalizing the results obtained for PEP–PEE-2, it is necessary to note that some aspects of its behavior are not universal. In a lamellar 12k–9k PS–PI diblock, Winey *et al.*[14] do not find a low-frequency regime of parallel alignment below the range where perpendicular alignment is observed. On the other hand, they find that parallel alignment occurs at a frequency well into the Rouse-like regime. In this regime, parallel alignment may be a consequence of the viscoelastic contrast between the lamellae and may require that chains not be entangled.

5.3. Mechanism of Parallel Alignment. The decay in the amplitudes of both σ_{12} and n_{12} during the parallel alignment process (Figure 6) can be described by a double exponential with time scales of approximately 480 s (~1.5 cycles) for the fast mode and 4000 s (~13 cycles) for the slow mode. During the first several hundred seconds, the stress and birefringence amplitudes decrease together and the stress–optic ratio SOR is essentially constant (Figure 7c). In contrast, the magnitude of the slow decay is much greater in n_{12} than in σ_{12}; this is manifested by a decrease in SOR (Figure 7c).

The large decrease in $|B^*_{eff}|$ while $|G^*_{eff}|$ is barely changing ($t > 4000$ s, Figures 7a,b) indicates that there exists a mode of dynamic response associated with a large dynamic birefringence per unit stress relative to the birefringence associated with distortion of chain conformation. This mode of dynamic response is eliminated progressively during flow alignment. The increase in the magnitude of the displacement of $n_{11} - n_{22}$ during the first 10 000 s is correlated with the decrease in the amplitude of n_{12}.[34] The development of the $n_{11} - n_{22}$ component of birefringence is consistent with the enhancement of parallel alignment determined previously by SANS.

One possible interpretation of the behavior of σ_{12}, n_{12}, and $n_{11} - n_{22}$ involves inhomogeneous deformation within a polydomain-ordered BCP, as has been observed in smectic liquid crystals.[30b] In layered liquids, two factors can give rise to inhomogeneous deformation: one is the variation in the local shear modulus due to variation in lamellar orientation, the other is the presence of focal conics that act as rigid structures suspended in the material. Due to the orientation dependence of the viscoelastic properties, oscillatory shear could produce a "wagging" or "rocking" of the lamellar normal, particularly the projection in the 1,2-plane. The amplitude of this rocking depends on the local orientation of the lamellae.

Over the course of one cycle, the rocking of the normal may not be completely reversed, as can be illustrated by considering a region with lamellar normal along the flow direction ($\hat{\mathbf{n}} \| \mathbf{v}$). As discussed above, such a region is rigid relative to the mean field around it, which initially consists of isotropically-oriented lamellar domains and various defect structures. The region with $\hat{\mathbf{n}} \| \mathbf{v}$ will behave initially like a rigid particle embedded in the medium and will rotate. As it rotates, its effective modulus decreases. This decrease in stiffness reduces the tendency of the domain to rotate rather than deform. At the end of the cycle the component of $\hat{\mathbf{n}}$ along $\mathbf{v}$ is less than unity, and the orientation distribution of the surrounding material is no longer isotropic. Due to both of these factors, the reverse cycle of strain does not produce a reversal in the trajectory of $\hat{\mathbf{n}}$. In particular, this region is expected to be less rigid than it was in its initial orientation, and smaller forces are expected to act on its periphery; therefore, this region is expected to rotate "back" to a lesser extent than it rotated "forward" during the first half-cycle of strain. Thus, the net effect of one cycle of strain is to reduce the component of $\hat{\mathbf{n}}$ along $\mathbf{v}$, increasing the component along the velocity gradient.

This picture of irreversible rocking can be applied to arbitrarily-oriented regions and used to explain progressive alignment induced by subsequent cycles of strain. This schematic view of the microrheology of parallel alignment is consistent with the decrease in dynamic birefringence n_{12} and its correlation with the increase in the displacement of $n_{11} - n_{22}$. Further, it is plausible that inhomogeneous deformation could produce a larger dynamic birefringence per unit of stress than is associated with the distortion of chain conformation, because the rocking of a whole domain

can contribute strongly to the birefringence for a small energy cost per unit volume, since only the material at the periphery is distorted. The monotonic decrease in the inhomogeneity of the deformation as alignment occurs is also consistent with the monotonic decrease in the stress–optic ratio, ultimately to the level associated with the distortion of chain conformation (Figure 7c). Comparison of the moduli at small strain (arrows at the margins of Figure 7a) with those observed at 90% strain shows that the nonlinear dependence on strain is modest for the conditions that produce parallel alignment. This is consistent with the flow being so slow that the microstructure is not highly perturbed, allowing domains to respond as dictated by their local orientation and immediate surroundings. Later this will be compared to the quite different behavior that leads to perpendicular alignment.

This conceived model is consistent with the observation of Bates and coworkers that a sample, having been previously aligned perpendicular, remains in the perpendicular alignment if it is subjected to a shearing that would produce parallel alignment of an initially isotropic sample. Since the present picture of the mechanism of parallel alignment involves the biased rocking of the projection of the layer normal in the 1,2-plane, it would have no effect on a sample that has $\hat{n}$ along the vorticity axis. Finally, it is consistent with the SANS patterns observed for parallel aligned samples, which showed that the parallel orientation is enhanced, but perpendicular alignment also remains. In the present view of the dynamics of parallel alignment, the projection of the layer normal along the vorticity axis is largely unaffected by the process. The presence of this orientation in the initial isotropic distribution is carried through to the final parallel aligned state.

The notion of irreversible rocking of grains does not address the detailed dynamics of defects in the system. Winey it et al. have shown that flow-induced alignment is associated with a reduction in the number of wall and focal conic defects in a lamellar diblock copolymer (SI 12/9).[13] While wall defects might be eliminated by rotation of adjacent domains, focal conic defects can be eliminated only by local rupture of lamellae. This indicates that "grain rotation" alone cannot completely explain the annihilation of defects that occurs during the process.

Regarding the possibility of relaxation upon cessation of flow, in PEP–PEE-2 when large-amplitude shearing is interrupted and resumed, the stress and birefringence responses resume with essentially the same amplitudes and displacement just as they had before the interruption. No evidence of relaxation has been observed. This is unlike the behavior reported recently[13] for a 12k–9k polystyrene–polyisoprene lamellar diblock copolymer in which the dynamic modulus recovers after cessation of shearing at an amplitude large enough to induce parallel alignment.[35]

5.4. Development of Perpendicular Alignment. At a frequency of 1 rad/s, the value of G' of the perpendicular state is more than 1 order of magnitude smaller than that of the unaligned state (Figure 4a), and the ratio of G'_{so}:G' is one-fifth as large as that in the unaligned material (Figures 3 and 5). This leads one to expect a 10-fold drop in G'_{eff} during flow alignment, and an even greater reduction in B'_{eff}. However, there is only a 4-fold decrease in G'_{eff}, and B'_{eff} and G'_{eff} decrease in a similar manner during the first 4000 s. The discrepancy between what is expected based on the small strain behavior ($\gamma_o \leq 2\%$) and what is observed during flow alignment can be understood in light of the strain dependence of B' and G'. During the very first cycle of large amplitude strain, G'_{eff} is immediately one-tenth as large as G' (shown by the arrow labeled G' on the vertical axis at $t = 0$). Almost all of the enhancement of G' due to the microstructure of the unaligned sample is lost at high strains. Consequently, the alignment of the microstructure has a much smaller effect on G'_{eff} (1 rad/s) $\gamma_o = 90\%$ than expected, based on G' (1 rad/s) ($\gamma_o \leq 2\%$). In relation to the notion that flow alignment is driven by the tendency of the fluid to minimize its resistance to flow, there is negligible driving force for alignment during this process.

In contrast to the parallel alignment process, during which the amplitude of n_{12} decreases much more than that of σ_{12}, the magnitude of the two decrease proportionately during perpendicular alignment (Figure 8a,b). The amplitude-based stress–optic ratio SOR during the process is nearly equal to C_{eff} determined at high frequency ($\omega > \omega'_{c,so}$) and small strain amplitude. This is expected because the stress is dominated by the loss component and the frequency of prolonged shear falls above ω''_{so} in the region where the loss modulus is dominated by molecular rather than microstructural relaxation (Figure 3); therefore, G''_{eff} and B''_{eff} are expected to be insensitive to flow alignment and remain proportional.

The magnitude of the displacement of $n_{11} - n_{33}$ increases with time, consistent with the SANS observation that similar conditions induce perpendicular alignment. The increase in $n_{11} - n_{33}$ also appears bimodal with a fast time scale of rougly 100 s and a slow time scale of ~400 s. The sharp initial rise in $n_{11} - n_{33}$ correlates with an abrupt drop in G'_{eff} and B'_{eff}. On the longer time scale, there is a significant increase in $n_{11} - n_{33}$, while G^*_{eff} and B^*_{eff} remain almost unchanged. That G^*_{eff} and B^*_{eff} are insensitive to lamellar alignment is consistent with the observation that both appear to be dominated by polymeric rather than microstructural contributions under the flow conditions that produce perpendicular alignment. Under such conditions, if the behavior of $n_{11} - n_{33}$ was not observed, the plateau in G^*_{eff} and B'_{eff} might be interpreted incorrectly as indicating that the alignment of the microstructure is no longer changing.

5.5. Static Birefringence of Aligned Samples. The magnitude of the $n_{11} - n_{33}$ birefringence in the perpendicular-aligned sample and the magnitude of the $n_{11} - n_{22}$ birefringence of the parallel-aligned sample are comparable to each other, with that of the perpendicular sample being somewhat higher than that of the parallel sample. This is consistent with earlier SANS results[5] showing that the degree of alignment is higher in perpendicular than in parallel PEP–PEE-2. Both aligned samples have static birefringence that is orders of magnitude smaller than an estimate of $\Delta n \approx 7 \times 10^{-4}$, based on analysis of strongly-segregated lamellar BCPs applied to the case of PEP–PEE-2.[20] As a result of the small refractive index difference between PEP and PEE ($n_{PEP} = 1.48$, $n_{PEE} = 1.487$), the intrinsic contribution dominates this birefringence (intrinsic:form ≈ 40:1). Since the static birefringence of PEP–PEE-2 is dominated by the segmental orientation distribution, the discrepancy between the theoretical and observed birefringence suggests that in the weakly-segregated conditions of our experiments the chains are much less oriented with respect to the interfaces of the lamellae than they would be in the strongly-segregated state assumed in the Lodge–Fredrickson analysis.

Indeed, recent simulations of the ordering transition of symmetric, diblock amphiphiles show that orientational order is very weak near the ODT.[36] For the longest diblocks simulated ($N = 48$), the orientational order parameter of

the chain segments was found to be $\bar{P}_2 = 6 \times 10^{-4}$. Since PEP–PEE-2 consists of 130 Kuhn segments, the simulations suggest $\bar{P}_2 = 8 \times 10^{-5}$ on the basis of the scaling $\bar{P}_2 \sim N^{-2}$ found in the simulations. This corresponds to a static birefringence of 3.8×10^{-6} for aligned lamellae, given the properties of PEP–PPE-2.[20] This result is in reasonable accord with our experimental observations (Figure 3).

6. Conclusion

This study demonstrates that stress–optical measurements can provide valuable information regarding both the effect of lamellar alignment on the dynamics of ordered BCPs and the development of the flow-induced alignment of their microstructure. In PEP–PEE-2 at conditions near the ODT, the behavior of the shear stress and birefringence during the process suggests that parallel alignment is associated with the irreversible rocking of domains in the material, while perpendicular alignment occurs under conditions in which the microscale deformation is essentially homogeneous. The selection of the direction of flow alignment of PEP–PEE-2 is not dictated by the orientation that minimizes the modulus, nor is the progress of alignment always manifested by a decrease in the magnitude of the shear stress. Both for parallel and perpendicular cases, much of the alignment is induced by a "fast" process on a time scale that is comparable to the period of the oscillatory shear. During this fast process the dynamic birefringence and stress decrease together. The degree of alignment improves further on a much longer time scale (an order of magnitude slower than the "fast" process), but this change is hardly manifested in the macroscopic mechanical properties.

Because these rheo-optical measurements are performed in real time, *in situ* they are well suited to screening many conditions of frequency and temperature in an efficient manner. Thus, it is natural to apply this approach to determine the crossover frequencies from one direction of alignment to another, the effect of χN on these crossover frequencies, and the characteristic time scales or strain scales that control the rate of alignment and their dependence on ω, γ_0 and χN. The influence of entanglement and viscoelastic contrast between the lamellae should also be explored, with the goal of understanding the differences in the observed behavior between PEP–PEE and PS–PI. These issues are central to understanding the mechanisms of flow alignment, which would ultimately permit the design of BCPs for applications or processing strategies that take advantage of flipping.

Acknowledgment. This research was carried out with the support of the NSF-PYI program (J.A.K.), with matching funds provided by AT&T. Acknowledgment is also made to the donors of the Petroleum Research Fund, administered by the American Chemical Society, for partial support of this research. We thank Frank Bates for providing PEP–PEE-2. We are grateful to Frank Bates, Ron Larson, and Scott Milner for enlightening discussions.

References and Notes

(1) Aggarwal, S. L., Ed. *Block Copolymers*; Plenum Press: New York, 1979.
(2) Bates, F. S.; Fredrickson, G. H. *Annu. Rev. Phys. Chem.* **1990**, *41*, 525.
(3) Bates, F. S. *Science* **1991**, *251*, 898.
(4) Leibler, L. *Macromolecules* **1980**, *13*, 1602.
(5) Koppi, K.; Tirrel, M.; Bates, F. S.; Almdal, K.; Colby, R. H. *J. Phys. II* **1992**, *2*, 1941.
(6) Koppi, K.; Tirrel, M.; Bates, F. S. *Phys. Rev. Lett.* **1993**, *70*, 1449.
(7) Keller, A.; Pedemonte, E.; Willmouth, F. M. *Colloid Polym. Sci.* **1970**, *238*, 25.
(8) Folkes, M. J.; Keller, A.; Scalisi, F. P. *Colloid Polym. Sci.* **1973**, *251*, 1.
(9) Hadziioannou, G.; Mathis, A.; Skoulios, A. *Colloid Polym. Sci.* **1979**, *257*, 15, 136, 344.
(10) Morrison, F. A.; Winter, H. H. *Macromolecules* **1989**, *22*, 3533.
(11) Morrison, F. A.; Winter, H. H.; Gronski, W.; Barnes, J. D. *Macromolecules* **1990**, *23*, 4200.
(12) Albalak, R. J.; Thomas, E. L. *J. Polym. Sci., Polym. Phys. Ed.* **1993**, *31*, 37.
(13) Winey, K. I.; Patel, S. S.; Larson, R. G.; Watanabe, H. *Macromolecules* **1993**, *26*, 2542.
(14) Winey, K. I.; Patel, S. S.; Larson, R. G.; Watanabe, H. *Macromolecules* **1993**, *26*, 4373.
(15) Amundson, K.; Helfand, E.; Davis, D. D.; Quan, X.; Patel, S. S.; Smith, S. D. *Macromolecules* **1991**, *24*, 6546.
(16) (a) Thomas, H. R.; O'Malley, J. J. *Macromolecules* **1979**, *12*, 323. (b) Hasegawa, H.; Hashimoto, T. *Macromolecules* **1985**, *18*, 589. (c) Coulon, G.; Russell, T. P.; Deline, V.; Green, P. F. *Macromolecules* **1989**, *22*, 2581.
(17) Amundson, K.; Helfand, E. *Macromolecules* **1993**, *26*, 1324.
(18) Bruinsma, R.; Rabin, Y. *Phys. Rev. A* **1992**, *45*, 994.
(19) Fuller, G. G. *Annu. Rev. Fluid Mech.* **1990**, *22*, 387.
(20) Lodge, T. P.; Fredrickson, G. H. *Macromolecules* **1992**, *25*, 5643.
(21) Janeschitz-Kriegl, H. *Polymer Melt Rheology and Flow Birefringence*; Springer: New York, 1983.
(22) Bates, F. S.; Rosedale, J. H.; Bair, H. E.; Russell, T. P. *Macromolecules* **1989**, *21*, 2557.
(23) Rosedale, J. H.; Bates, F. S. *Macromolecules* **1990**, *23*, 2329.
(24) Johnson, S. J.; Frattini, P. L.; Fuller, G. G. *J. Colloid Interface Sci.* **1985**, *104*, 440.
(25) Kannan, R. M.; Kornfield, J. A. *Rheol. Acta* **1992**, *31*, 535.
(26) Kannan, R. M.; Kornfield, J. A.; Schwenk, N.; Boeffel, C. *Macromolecules* **1993**, *26*, 2050.
(27) As the strain γ_0 is increased, the higher-order harmonics (3ω, 5ω, etc.) may become important in the shear stress and the description of σ_{12} by G^*_{eff} will fail. Similarly, it will not be possible to describe n_{12} completely in terms of B^*_{eff} when γ_0 is so large that higher-order harmonics become significant.
(28) The complex birefringence coefficient B^* used here is to the complex mechano-optic coefficient S^* of Lodge and Lodge[29] as the dynamic modulus G^* is to the complex viscosity η^*.
(29) Lodge, T. P.; Lodge, S. A. *Rheol. Acta* **1992**, *31*, 32.
(30) (a) Larson, R. G.; Winey, K. I.; Patel, S. S.; Watanabe, H.; Bruinsma, R. *Rheol. Acta* **1993**, *32*, 245. (b) Viscoelastic measurements and video-microscopic recording of the behavior of the small-molecule smectic 8CB using rheo-microscopy (presented by Ron Larson at the Society of Rheology Meeting, February 1993).
(31) Kawasaki, K.; Onuki, A. *Phys. Rev. A* **1990**, *42*, 3664.
(32) Presentation "Toward an Understanding of Flow-Alignment of Block-Copolymers" by Scott Milner and Glen Fredrickson at the 2nd International Meeting on Relaxations in Complex Systems, Alicante, Spain, 1993.
(33) One would expect that there is a single characteristic time scale that underlies each pair of critical frequencies (ω_c', ω_c'') and $(\omega_{c,so}', \omega_{c,so}'')$, because the dynamic moduli are associated with a single underlying relaxation function, and assuming that each pair is associated with a particular mode of relaxation. Indeed, the difference between ω_c' and ω_c'' is small enough that it can be attributed to the fact that changes in the near terminal part of the relaxation spectrum are manifested more strongly in G' than in G'', so they are perceptible at a higher frequency in G' than in G''. However, the difference between $\omega_{c,so}'$ and $\omega_{c,so}''$ is much larger. This suggests that they arise from different dynamic modes of the polydomain BCP.
(34) At still longer times ($t > 10\,000$ s), there appears to be significant baseline drift; therefore, further experiments are required to determine the behavior of $n_{11} - n_{22}$ from 10 000 to 25 000 s.
(35) The reduction in modulus observed in PS-PI 12k/9k has recently been attributed to melt fracture and its recovery due to "healing" of the sample (R. G. Larson's lecture on melt fracture at the AIChE meeting, November 1993).
(36) Larson, R. G. Simulation of Lamellar Phase Transitions in Block Copolymers and Surfactants. *Mol. Simulation*, submitted for publication.